Showcasing research from Professor Stefan Bräse's laboratory, Institute of Organic Chemistry (IOC), Karlsruhe Institute of Technology (KIT), Karlsruhe, Germany. Vincenzo Pani is acknowledged for the creation of the image.

Modulating the photolysis of aryl azides in a supramolecular host to develop photoactivatable fluorophores

Photolysis of aryl azides within the supramolecular host cucurbit[7]uril occurs through a controlled reaction pathway, leading to photoactivatable fluorescence, which has been successfully utilized for bioimaging applications.

As featured in:

See Ute Schepers, Stefan Bräse *et al.*, *Chem. Commun.*, 2024, **60**, 12856.

ROYAL SOCIETY OF CHEMISTRY

rsc.li/chemcomm

Registered charity number: 207890

ChemComm

COMMUNICATION

View Article Online
View Journal | View Issue

Cite this: *Chem. Commun.*, 2024, **60**, 12856

Received 1st August 2024,
Accepted 2nd October 2024

DOI: 10.1039/d4cc03907f

rsc.li/chemcomm

Modulating the photolysis of aryl azides in a supramolecular host to develop photoactivatable fluorophores†

Xujun Qiu,‡[a] Eric Pohl,‡[b] André Jung,[c] Qianyu Cai,[a] Haopu Su,[a] Olaf Fuhr,[de] Ute Schepers*[ab] and Stefan Bräse*[ac]

Photolysis of aryl azides is a convenient method to approach more functionalized systems in chemical biology. Here, we present a set of photoactivatable aryl azides that undergo controlled reaction pathways within the cucurbit[7]uril (CB7) cavity upon photolysis. The fluorescence turn-on process is utilized for bioimaging.

Photoconvertible molecules which can undergo precisely directed photoreactions, significantly enhancing the emission from a weak or non-fluorescent state, are highly demanded.[1,2] This 'turn-on' process can be utilized for tracking the biological activity and real-time localization imaging.[3,4] Organic azides have shown their versatile applications in chemical biology, as they can be easily functionalized using various methods.[5,6] Photolysis of aryl azides is of crucial importance in chemical biology, with applications like light-induced protein labeling[7,8] and RNA photo-crosslinking.[9] Nevertheless, applications of aryl azides in living cells as photoactivatable probes are seldomly documented.[10–13] One possibility is the generation of highly toxic singlet nitrene during photolysis of aryl azides, reducing cell viability. Additionally, singlet nitrenes may undergo uncontrollable photoreaction pathways, leading to undesirable products.[14]

To overcome these challenges, we previously developed a novel method to selectively control the aryl azide photoreaction pathway to a carboline with dramatically enhanced fluorescence by implementing the photoreaction within the cavity of a macrocyclic molecule, cucurbit[7]uril (CB7).[15]

In this study, we designed and synthesized three aryl azides with a push–pull system. We demonstrated control over the photoreaction within the cavity of CB7, transforming low emission aryl azides into highly fluorescent carbolines. Time-dependent density functional theory (TD-DFT) calculations were used to study the mechanism of this 'turn-on' process. Additionally, we successfully applied the photoactivation process to living cells for optical imaging (Scheme 1).

We applied various electron-donating groups to the designed azides to modulate intramolecular charge transfer (ICT) and to adjust their absorption properties.[16] The syntheses and structures of aryl azides **Az-1**, **Az-2**, and **Az-3** are shown in Fig. 1, with full characterization in the ESI† (Fig. S1–S11 and Tables S1, S2). Photolysis of these azides was initially investigated in water using 405 nm LEDs (M405L4 – 405 nm, 1000 mW (Min) Mounted LED, 1000 mA, THORLABS) at room temperature. As indicated by the NMR spectra (Fig. S12, S14 and S16, ESI†), new peaks appeared after photolysis of **Az-1**, **Az-2**, and **Az-3**. Liquid chromatography-mass spectrometry (LC-MS) analysis of the reaction mixtures of **Az-1** and **Az-2** (Fig. S13 and S15, ESI†) revealed product masses of 348.23 g mol^{-1} for **Az-1** and 350.27 g mol^{-1} for **Az-2**. Compared to the starting masses of **Az-1** (376.26 g mol^{-1}) and **Az-2** (378.28 g mol^{-1}), these new masses indicate the formation of carboline products through photoreaction. This can be attributed to the highly hydrophobic aromatic ring conjugation in **Az-1** and **Az-2**, which promotes the molecule aggregation in water, forming noncovalent stacked systems.[17,18] These systems prevent water from attacking, leading to intramolecular C–H amination. The crystal packing structures of **Az-1** and **Az-2** further support this hypothesis (Fig. S4 and S8, ESI†).

In contrast, **Az-3**, which has a smaller aromatic conjugate, was found to form various products after irradiation. This was

[a] *Institute of Organic Chemistry (IOC), Karlsruhe Institute of Technology (KIT), Kaiserstrasse 12, 76131 Karlsruhe, Germany. E-mail: ute.schepers@kit.edu, braese@kit.edu*
[b] *Institute of Functional Interfaces (IFG), Karlsruhe Institute of Technology (KIT), Kaiserstrasse 12, 76131 Karlsruhe, Germany*
[c] *Institute of Biological and Chemical Systems - Functional Molecular Systems (IBCS-FMS), Karlsruhe Institute of Technology (KIT), Kaiserstrasse 12, 76131 Karlsruhe, Germany*
[d] *Institute of Nanotechnology (INT), Karlsruhe Institute of Technology (KIT), Kaiserstrasse 12, 76131 Karlsruhe, Germany*
[e] *Karlsruhe Nano Micro Facility (KNMFi), Karlsruhe Institute of Technology (KIT), Kaiserstrasse 12, 76131 Karlsruhe, Germany*

† Electronic supplementary information (ESI) available. CCDC 2351099 and 2351100. For ESI and crystallographic data in CIF or other electronic format see DOI: https://doi.org/10.1039/d4cc03907f

‡ These authors contributed equally.

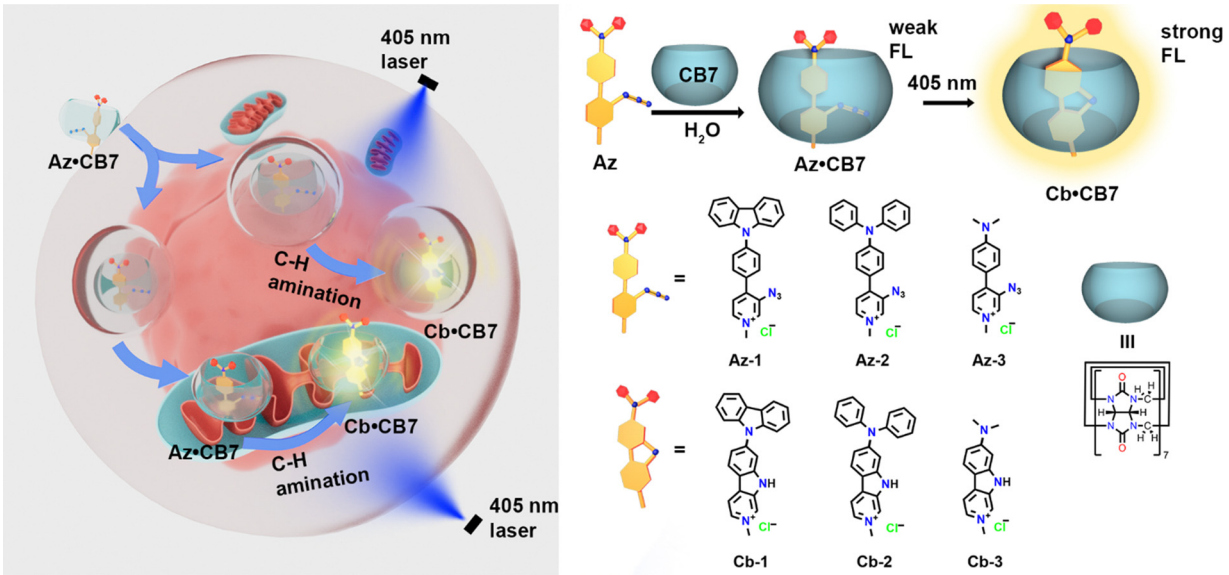

Scheme 1 Illustration of photoactivatable aryl azides' 'turn-on' emission in CB7 (left) and structures of azides and carbolines (right).

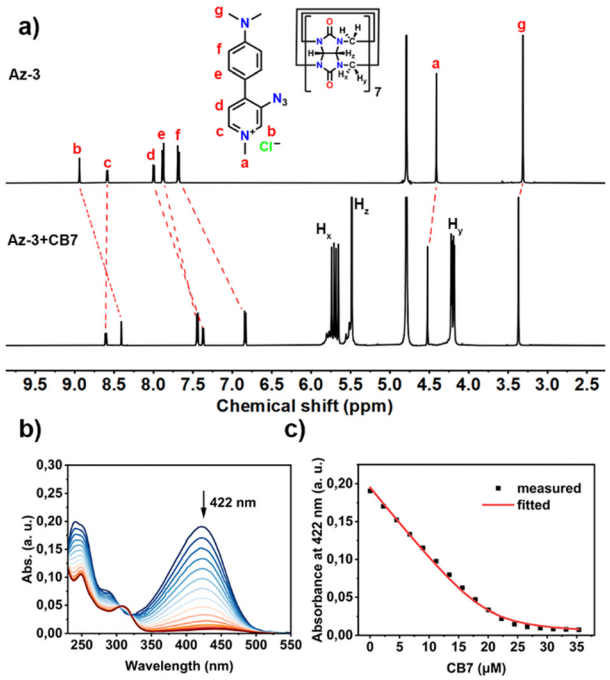

Fig. 1 (a) ^{1}H NMR spectra (500 MHz, D_2O) of **Az-3** (0.5 mM) and **Az-3** + CB7 (0.5 mM each); (b) UV-vis titration spectra of **Az-3** (20 μM) upon addition of CB7 (0–35 μM) in water at 298 K, and (c) the binding isotherm fitted with a 1 : 1 host–guest binding model.

evidenced by the presence of methyl groups in the resulting NMR spectra (Fig. S16, ESI†). LC–MS also revealed that the photolysis of **Az-3** in water produces a mixture of photoproducts with different molecular masses (Fig. S17, ESI†). The photoreaction processes were further monitored using UV-vis and emission spectra (Fig. S18–S20, ESI†), which suggest the reaction completes at 420 s for **Az-1**, 240 s for **Az-2** and 180 s for **Az-3**.

We then investigated the host–guest interaction of the synthesized aryl azides with CB7 using NMR techniques. As shown in Fig. S21–S23 (ESI†), the addition of CB7 to the **Az-1** solution resulted in significant proton shifts, whereas signals d and e exhibited an upfield shift, suggesting the deep encapsulation of azido moieties within CB7 cavities. The formation of a 1 : 1 complex of **Az-1** with CB7 was also observed by MALDI-TOF-MS (Fig. S24, ESI†), which showed a peak of *m*/*z* 1510.21 corresponding to [**Az-1**+CB7-Cl]$^{+}$ ions. The deep encapsulation within the CB7 cavity was also observed for **Az-2** and **Az-3** (Fig. 1(a) and Fig. S25–S32, ESI†).

The binding constants of the aryl azides and CB7 were determined by UV-vis titration (Fig. S33–S38, ESI†). The addition of CB7 to aryl azides resulted in a decrease in absorption intensity at 368 nm for **Az-1** (Fig. S33, ESI†), 422 nm for both **Az-2** (Fig. S35, ESI†) and **Az-3** (Fig. 1(b) and Fig. S37, ESI†). The binding constants were obtained by non-linear fitting, which were calculated to be $(3.79 \pm 0.18) \times 10^5$ M^{-1} for **Az-1** (Fig. S34, ESI†), $(1.76 \pm 0.05) \times 10^5$ M^{-1} for **Az-2** (Fig. S36, ESI†), and $(1.40 \pm 0.03) \times 10^6$ M^{-1} for **Az-3** (Fig. 1(c) and Fig. S38, ESI†). These values are comparable to those of previously studied aryl azides.[15]

Furthermore, the photoreaction of aryl azides within the CB7 cavities was performed under the same conditions as in water. As shown in Fig. S39–S56 (ESI†), the formation of carbolines through tuned intramolecular C–H amination within the CB7 cavities was observed. The resulting carbolines were characterized as shown in Fig. S42–S44 (ESI†) for **Cb-1**, Fig. S48–S50 (ESI†) for **Cb-2**, and Fig. S54–S56 (ESI†) for **Cb-3**. LC–MS revealed molecular masses of 348.23 g mol^{-1} for **Cb-1** (Fig. S41, ESI†), 350.27 g mol^{-1} for **Cb-2** (Fig. S47, ESI†), and 226.23 g mol^{-1} for **Cb-3** (Fig. S53, ESI†). The reaction progress was also tracked by UV-vis and emission spectroscopy, which suggest the carbolines formed within 240 s for **Cb-1** (Fig. S57, ESI†), 100 s for **Cb-2** (Fig. S58, ESI†), and 180 s for **Cb-3** (Fig. S59, ESI†).

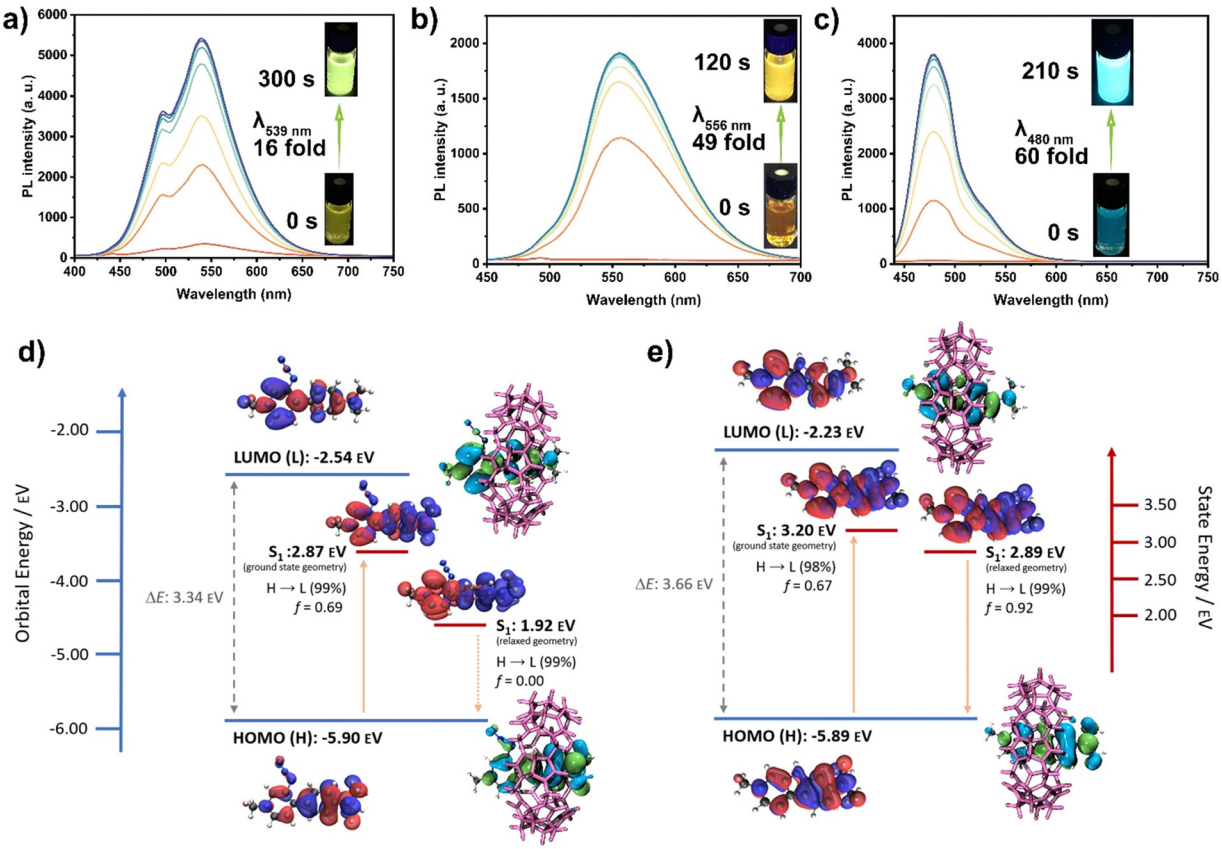

Fig. 2 Photoluminescence (PL) spectra of photolysis of (a) **Az-1**·CB7; (b) **Az-2**·CB7; and (c) **Az-3**·CB7 after different reaction times; (d) and (e) computed molecular orbitals (HOMO/LUMO) and difference density plots of the first excited singlet state at the ground state and relaxed S_1 geometry of **Az-3** and **Cb-3**, calculated at the (TD-)DFT PBE0/6-31+G(d,p)//B3LYP/6-31G(d) level of theory in water (PCM).

Interestingly, the emission spectra of the photoreaction products showed substantial increases in intensity. For **Cb-1**·CB7, the emission intensity at λ_{539nm} increased 16-fold compared to the weak emission of **Az-1**·CB7 (Fig. 2(a)). **Cb-2**·CB7 exhibited a 49-fold enhancement at λ_{556nm}, while **Cb-3**·CB7 showed a 60-fold enhancement at λ_{480nm} compared to the barely fluorescent **Az-2**·CB7 (Fig. 2(b)) and **Az-3**·CB7 (Fig. 2(c)). The photophysical properties of the carbolines are shown in Table S3 (ESI†), with photoreaction quantum yields of 16.3%, 31.4%, and 25.6% for **Az-1**, **Az-2**, and **Az-3** in CB7, respectively.

To better understand the nature of the fluorescence enhancement upon carboline formation, particularly the cyclization of **Az-3** to **Cb-3** within CB7, we performed DFT calculations (Fig. 2(d), (e) and Fig. S62, S63, ESI†). The highest occupied molecular orbital (HOMO) and lowest unoccupied molecular orbital (LUMO) orbital energies of azides and carbolines were compared, which are shown in Fig. 2(d), (e) and Fig. S62 (ESI†). The calculated results reveal similar bandgaps of carbolines and corresponding azides. For **Az-3**·CB7 and **Cb-3**·CB7 (Fig. 2(d) and (e)), hole and electron wavefunctions are distributed within the whole molecule at the ground state geometry. At the relaxed excited state geometry, hole and electron wavefunctions exhibit near-complete separation, which likely causes the S_1 state of **Az-3**·CB7 to become non-emissive. This is further supported by the near-zero oscillator strength observed in the system. In general, the state energies of the excited singlet states S_1 for azides were found to be lower than the corresponding carbolines. Additionally, absorption and emission spectra were simulated (Fig. S63, ESI†), revealing acceptable agreement with experimental results. The non-emissive nature of **Az-1** and **Az-2** could not be described *via* TD-DFT (Fig. S62, ESI†). However, the shortcomings of TD-DFT concerning the accurate description of (long-range) CT states are well known.[19,20]

Considering these findings, we explored this fluorescence photoactivation process for live cell imaging. Emission experiments performed in cell media showed enhanced fluorescence intensity for azide–CB7 complexes compared to their free forms (Fig. S64, ESI†). Following the photoreaction, emission intensities increased for both unbound and CB7-complexed carbolines (Fig. S65, ESI†). Interestingly, the PL intensities of **Cb-1** and **Cb-2** were higher than those observed within the CB7 cavity (Fig. S65, ESI†), likely due to large aromatic structures fitting into protein pockets in serum and reducing water quenching. In contrast, CB7 effectively shields the smaller **Cb-3** from water-based quenching. To verify this hypothesis, we tested the photophysical properties of **Cb-1**, **Cb-2**, **Cb-3**, and their CB7 complexes in the presence of bovine serum albumin (BSA), the most abundant protein in HeLa cell medium[21] and varying concentrations of fetal bovine serum (FBS) (Fig. S66–S83, ESI†).

We evaluated the cytotoxicity of aryl azides, carboline products, and their CB7 complexes on HeLa cells at different

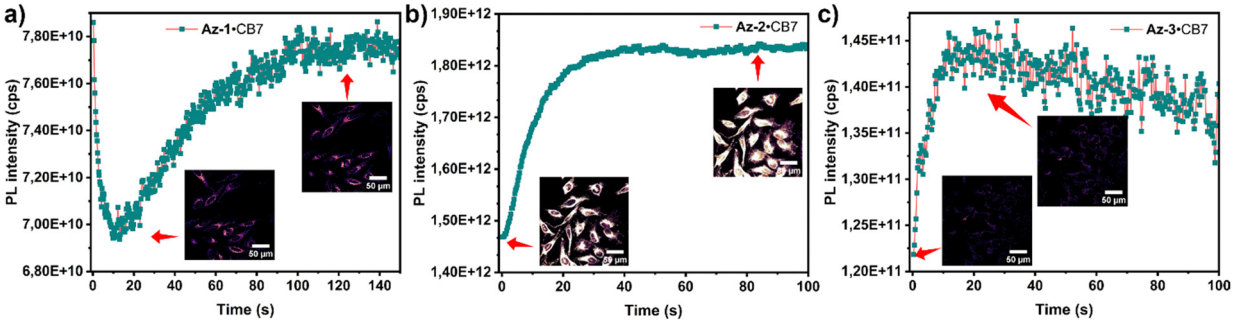

Fig. 3 PL intensity and confocal imaging of (a) **Az-1**·CB7; (b) **Az-2**·CB7; and (c) **Az-3**·CB7 upon reaction in HeLa cells.

concentrations (50 μM, 5 μM, and 0.5 μM) (Fig. S67, ESI†). Both aryl azides and carbolines exhibit similarly low cytotoxicity (LC50 > 50 μM). We then implemented azide–CB7 complexes in living cells, followed by photoactivation. As shown in Fig. 3, fluorescence intensity increased after irradiation, indicating intracellular carboline formation. Photoreaction without CB7 led to faster reaction times and reduced PL for azides, highlighting the role of CB7 in enhancing cellular uptake and directing the photoreaction (Fig. S68, ESI†). Additionally, we preactivated azides·CB7 to carbolines in cell media, prior to the uptake for imaging (Fig. S69a, ESI†). As shown in Fig. S69b (ESI†), carboline–CB7 complexes **Cb-1**·CB7 and **Cb-2**·CB7 were accumulated within endosomal vesicles, while **Cb-3**·CB7 was predominantly found in mitochondria. We cultivated cells with carboline–CB7 complexes under light exposure to assess long-term effects and biocompatibility, revealing no significant cytotoxicity (Fig. S84, ESI†).

In summary, we developed a novel approach for developing photoactivatable fluorescent probes utilizing the CB7 host to control the photoreaction pathway of aryl azides into carbolines, resulting in a significantly enhanced fluorescence intensity. DFT calculations elucidated the fluorescence 'turn-on' mechanism. Besides, we successfully applied this photoactivation process in live cell imaging, highlighting the potential of controlling aryl azide photolysis within supramolecular hosts for biochemical applications.

The supports from China Scholarship Council, bwHPC, Deutsche Forschungsgemeinschaft (DFG) under Germany's Excellence Strategy-3DMM2O-EXC-2082/1-390761711, and INST 40/575-1 FUGG (Justus 2 cluster) are gratefully acknowledged. Prof. H.-A. Wagenknecht (IOC, KIT) and Dr F. Biedermann (INT, KIT) are gratefully acknowledged for access to photophysics equipment used in this study.

Data availability

Data for this article, including NMR and IR, are available at Chemotion Repository at **https://www.chemotion-repository.net/welcome** *via* the DOI in the ESI.†

Conflicts of interest

There are no conflicts to declare.

Notes and references

1 X. Gu, E. Zhao, T. Zhao, M. Kang, C. Gui, J. W. Y. Lam, S. Du, M. M. T. Loy and B. Z. Tang, *Adv. Mater.*, 2016, **28**, 5064–5071.
2 Q. Gong, X. Zhang, W. Li, X. Guo, Q. Wu, C. Yu, L. Jiao, Y. Xiao and E. Hao, *J. Am. Chem. Soc.*, 2022, **144**, 21992–21999.
3 C. Xu, H. Zou, L. Hu, H. Shen, H. H. Y. Sung, H. Feng, R. T. K. Kwok, J. W. Y. Lam, L. Zheng and B. Z. Tang, *ACS Mater. Lett.*, 2022, **4**, 1831–1839.
4 K. Kikuchi, L. D. Adair, J. Lin, E. J. New and A. Kaur, *Angew. Chem., Int. Ed.*, 2023, **62**, e202204745.
5 C. Bednarek, I. Wehl, N. Jung, U. Schepers and S. Bräse, *Chem. Rev.*, 2020, **120**, 4301–4354.
6 N. Z. Fantoni, A. H. El-Sagheer and T. Brown, *Chem. Rev.*, 2021, **121**, 7122–7154.
7 Y. Zhang, J. Tan and Y. Chen, *Chem. Commun.*, 2023, **59**, 2413–2420.
8 N. E. S. Tay, K. A. Ryu, J. L. Weber, A. K. Olow, D. C. Cabanero, D. R. Reichman, R. C. Oslund, O. O. Fadeyi and T. Rovis, *Nat. Chem.*, 2023, **15**, 101–109.
9 K. L. Buchmueller, B. T. Hill, M. S. Platz and K. M. Weeks, *J. Am. Chem. Soc.*, 2003, **125**, 10850–10861.
10 S. J. Lord, N. R. Conley, H.-L. D. Lee, R. Samuel, N. Liu, R. J. Twieg and W. E. Moerner, *J. Am. Chem. Soc.*, 2008, **130**, 9204–9205.
11 A. V. Anzalone, Z. Chen and V. W. Cornish, *Chem. Commun.*, 2016, **52**, 9442–9445.
12 S. H. Liyanage, N. G. H. Raviranga, J. G. Ryan, S. S. Shell, O. Ramström, R. Kalscheuer and M. Yan, *JACS Au*, 2023, **3**, 1017–1028.
13 X. Qiu, E. Pohl, Q. Cai, J. Seibert, Y. Li, S. Leopold, O. Fuhr, M. A. R. Meier, U. Schepers and S. Bräse, *Adv. Funct. Mater.*, 2024, 2401938.
14 M.-L. Tsao, N. Gritsan, T. R. James, M. S. Platz, D. A. Hrovat and W. T. Borden, *J. Am. Chem. Soc.*, 2003, **125**, 9343–9358.
15 X. Qiu, Y. Wang, S. Leopold, S. Lebedkin, U. Schepers, M. M. Kappes, F. Biedermann and S. Bräse, *Small*, 2024, **20**, 2307318.
16 A. Slama-Schwok, M. Blanchard-Desce and J. M. Lehn, *J. Phys. Chem.*, 1990, **94**, 3894–3902.
17 K. Leduskrasts, A. Kinens and E. Suna, *Chem. Commun.*, 2019, **55**, 12663–12666.
18 H. Park, G. Niu, C. Wu, C. Park, H. Liu, H. Park, R. T. K. Kwok, J. Zhang, B. He and B. Z. Tang, *Chem. Sci.*, 2022, **13**, 2965–2970.
19 M. Campetella, F. Maschietto, M. J. Frisch, G. Scalmani, I. Ciofini and C. Adamo, *J. Comput. Chem.*, 2017, **38**, 2151–2156.
20 T. Froitzheim, S. Grimme and J.-M. Mewes, *J. Chem. Theory Comput.*, 2022, **18**, 7702–7713.
21 S. Curry, H. Mandelkow, P. Brick and N. Franks, *Nat. Struct. Mol. Biol.*, 1998, **5**, 827–835.